Electronic phase diagram of high-temperature copper oxide superconductors

Utpal Chatterjee[a,b], Dingfei Ai[a], Junjing Zhao[a], Stephan Rosenkranz[b], Adam Kaminski[c], Helene Raffy[d], Zhizhong Li[d], Kazuo Kadowaki[e], Mohit Randeria[f], Michael R. Norman[b], and J. C. Campuzano[a,b,1]

[a]Department of Physics, University of Illinois at Chicago, Chicago, IL 60607; [b]Materials Science Division, Argonne National Laboratory, Argonne, IL 60439; [c]Ames Laboratory and Department of Physics and Astronomy, Iowa State University, Ames, IA 50011; [d]Laboratorie de Physique des Solides, Universite Paris-Sud, 91405 Orsay Cedex, France; [e]Institute of Materials Science, University of Tsukuba, Ibaraki 305, Japan; and [f]Department of Physics, The Ohio State University, Columbus, OH 43210

Edited by J. C. Seamus Davis, Cornell University, Ithaca, NY, and approved April 25, 2011 (received for review February 2, 2011)

In order to understand the origin of high-temperature superconductivity in copper oxides, we must understand the normal state from which it emerges. Here, we examine the evolution of the normal state electronic excitations with temperature and carrier concentration in $Bi_2Sr_2CaCu_2O_{8+\delta}$ using angle-resolved photoemission. In contrast to conventional superconductors, where there is a single temperature scale T_c separating the normal from the superconducting state, the high-temperature superconductors exhibit two additional temperature scales. One is the pseudogap scale T^*, below which electronic excitations exhibit an energy gap. The second is the coherence scale T_{coh}, below which sharp spectral features appear due to increased lifetime of the excitations. We find that T^* and T_{coh} are strongly doping dependent and cross each other near optimal doping. Thus the highest superconducting T_c emerges from an unusual normal state that is characterized by coherent excitations with an energy gap.

cuprates | photoelectron spectroscopy

General features of the phase diagram of the copper oxide superconductors have been known for some time. The superconducting transition temperature T_c has a dome-like shape in the doping-temperature plane with a maximum near a doping $\delta \sim 0.167$ electrons per Cu atom. Although in conventional metals the electronic excitations for $T > T_c$ are (*i*) gapless and (*ii*) sharply defined at the Fermi surface (1), the cuprates violate at least one of these conditions over much of their phase diagram. These deviations from conventional metallic behavior are most easily described in terms of two energy scales T^* (2, 3) and T_{coh} (4), which correspond to criteria (*i*) and (*ii*), respectively.

To address the role of these energy scales in defining the phase diagram, we concentrate on spectra where the superconducting energy gap is largest, the antinode [$(\pi,0) \rightarrow (\pi\pi)$ Fermi crossing], where the spectral changes with doping and temperature are most pronounced (the *SI Appendix* has further details). Spectral changes at the node have been previously studied by Valla et al. (5) and such spectra remain gapless for all doping values (6). In Fig. 1, we show spectra at fixed temperature as a function of doping. Data points are indicated in Fig. 1*A* (See *SI Appendix* for experimental conditions and sample details). Initially, we show spectra at fixed momenta as a function of energy (energy distribution curves, or EDCs) that have been symmetrized (7) about the Fermi energy to remove the effects of the Fermi function. Later, we show that equivalent results are obtained from division of the EDCs by a resolution-broadened Fermi function. In the following figures, because two values of the doping can result in the same T_c, samples are labeled as OP for optimally doped, OD for overdoped, and UD for underdoped.

The spectra at the antinode at the highest temperature (approximately 300 K) in Fig. 1*D* show two remarkable features: They are extremely broad in energy, exceeding any expected thermal broadening, and their line shapes, well described by a Lorentzian, are independent of doping. The large spectral widths indicate electronic excitations that cannot be characterized by a well-defined energy, implying that the electrons are strongly interacting.

The incoherent behavior of the spectra at 300 K is consistent with the strange metal regime in two model phase diagrams popular in the literature, shown schematically in Fig. 1 *B* and *C*. If Fig. 1*B* applies, there would be strong evidence for a single quantum critical point near optimal doping which dominates the behavior to high temperatures (8, 9). T^* would be the transition temperature for a competing order, with T_{coh} its "mirror" corresponding to where Fermi liquid behavior sets in. The non-Fermi liquid behavior in the strange metal phase above both scales would then arise from fluctuations in the quantum critical region (10). These same fluctuations presumably mediate superconducting pairing. On the other hand, if Fig. 1*C* applies, the phase diagram would arise from strong correlation theories based on doped Mott insulators (11–14). The T^* line is where spin excitations become gapped, whereas T_{coh} is the temperature below which doped carriers become coherent. Superconductivity emerges below both scales, where spin and charge excitations become gapped and coherent. Which of these two phase diagrams is the appropriate one has critical implications for our understanding of the cuprates. To study this, we reduce T. At approximately 150 K, the spectra show marked changes with doping, and three regions can be identified in Fig. 1*E*. At low δ, the spectrum (red curve) remains broad as in Fig. 1*D*, but now a spectral gap is present—the pseudogap. This results in a reduction of the low-energy spectral weight as probed by various experiments (15). On increasing δ, the spectral gap becomes less pronounced and disappears just below optimal doping (purple and brown curves), where the spectra now resemble those in Fig. 1*D*. Increasing δ beyond 0.17, the spectra exhibit a sharp peak centered at zero energy (E_F) (blue and green curves). It can be seen in Fig. 1*E* that the sharper portion of the latter two spectra rises above the Lorentzian part of the spectrum delineated by the purple curve. These sharp spectra are now similar to what one would expect for a more conventional metal (1, 16). The doping dependences near 150 K are again consistent with either Fig. 1 *B* or *C*.

A completely different behavior emerges at a lower temperature, 100 K (Fig. 1*F*). The pseudogap with no sharp peaks is still present for low δ (red and purple curves). But near optimal doping, the spectra change, now exhibiting sharp peaks separated by an energy gap (brown, blue, and light-blue curves). These

Author contributions: U.C. and J.C.C. designed research; U.C., D.A., J.Z., S.R., A.K., H.R., Z.L., and K.K. performed research; U.C., S.R., A.K., M.R.N., and J.C.C. analyzed data; H.R., Z.L., and K.K. grew the samples; and U.C., M.R., M.R.N., and J.C.C. wrote the paper.

The authors declare no conflict of interest.

This article is a PNAS Direct Submission.

Freely available online through the PNAS open access option.

[1]To whom correspondence should be addressed. E-mail: jcc@uic.edu.

This article contains supporting information online at www.pnas.org/lookup/suppl/doi:10.1073/pnas.1101008108/-/DCSupplemental.

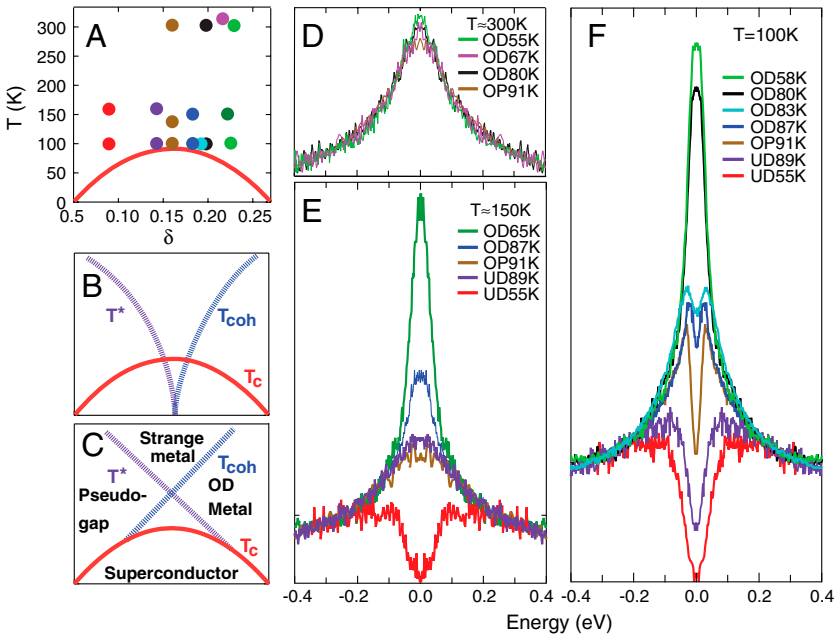

Fig. 1. Spectra at constant temperature as a function of doping. (*A*) Dots indicate the temperature and doping values of the spectra of the same color plotted in *D*–*F*. (*B*) Schematic phase diagram for a quantum critical point near optimal doping. (*C*) Schematic phase diagram for a doped Mott insulator. (*D*) Spectra at $T \sim 300$ K for several samples measured at the antinode, where the *d*-wave superconducting gap below T_c is largest. The spectra are normalized to high binding energy and symmetrized in energy to eliminate the Fermi function. The doping values are indicated by the top row of dots in *A*. (*E*) Same as in *D*, but at $T \sim 150$ K, with the dopings indicated by the middle row of dots in *A*. (*F*) Same as in *D*, but at $T = 100$ K, with the dopings indicated by the bottom row of dots in *A*.

sharp peaks indicate that the lifetimes of excitations have increased dramatically, in contrast to the spectra at 150 K for optimal doping (brown curve in Fig. 1*E*). For still higher δ, a single sharp peak centered at E_F appears (green and black curves). Notice that all the spectral changes are limited to an energy scale of less than 200 meV; outside this energy range, the spectra follow the same broad Lorentzian shape as in Fig. 1*D*.

Fig. 1*F* demonstrates that the spectral gap and coherence (manifested by sharp spectral peaks) coexist in the normal state near optimal doping, implying that the T^* and $T_{\rm coh}$ lines cross each other, as in Fig. 1*C*. To further illustrate this crossing, we plot spectra at fixed doping as a function of temperature, with the various data points indicated in Fig. 2*A*. Fig. 2*B* shows spectra for two optimally doped samples. At $T = 90$ K (light-blue curve), the sample is just emerging from the superconducting state. Increasing T, the sharp peaks at the edge of the gap decrease in intensity, whereas the gap magnitude remains constant. Finally, for $T \geq 115$ K (pink curve), the sharp peaks disappear, whereas the spectral gap remains. This indicates that the $T_{\rm coh}$ line has been crossed, but not the T^* line. For $T \geq 138$ K (red curve), the spectral gap has completely filled in, and the spectra have regained the broad, temperature-independent line shape characteristic of the strange metal phase of Fig. 1*D*.

In contrast, upon increasing the doping, the crossing of the pseudogap and coherence temperatures are reversed, as illustrated in Fig. 2*C*. Starting in the superconducting state at 66 K (blue curve), one can see the same features as in Fig. 2*B*, but now the spectral gap is smaller. Once T_c is crossed at 90 K, the spectral gap and sharp peaks persist (green and brown curves). But at higher T, the gap disappears and we are left with a relatively sharp peak at E_F (red curve), in contrast to Fig. 2*B*. For higher temperatures, the peaks broaden as in Fig. 1*D*. If the doping is now increased even further (Fig. 2*D*), a spectral gap is no longer observed at any $T > T_c$. In this highly overdoped region, the superconducting transition is similar to that of conventional superconductors (1), as the spectral gap closes very near T_c. The peak at E_F initially remains sharp, but at high enough temperatures, the strange metal returns (purple, red, and violet curves).

In Fig. 3, we show that dividing the EDCs by a resolution-broadened Fermi function (17) gives equivalent results to symmetrizing them. To quantitatively determine the T^* line, we note that it is easily identified by where the spectral gap disappears (18).

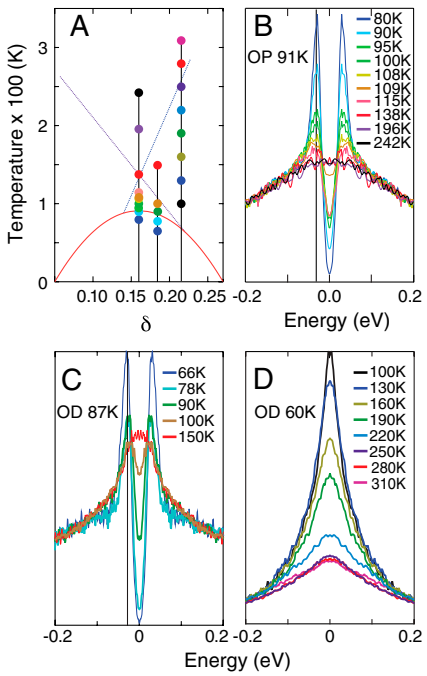

Fig. 2. Spectra at constant doping as a function of temperature. (*A*) Dots indicate the temperature and doping values of the spectra of the same color plotted in *B*–*D*. (*B*) Symmetrized antinodal spectra for two optimally doped samples ($\delta = 0.16$). The temperature values are indicated by the left row of dots in *A*. (*C*) Same as in *B*, but for a doping of $\delta = 0.183$, with the temperatures indicated by the middle row of dots in *A*. (*D*) Same as in *B*, but for a doping of $\delta = 0.224$, with the temperatures indicated by the right row of dots in *A*. Gray lines in *B* and *C* mark the location of the gap.

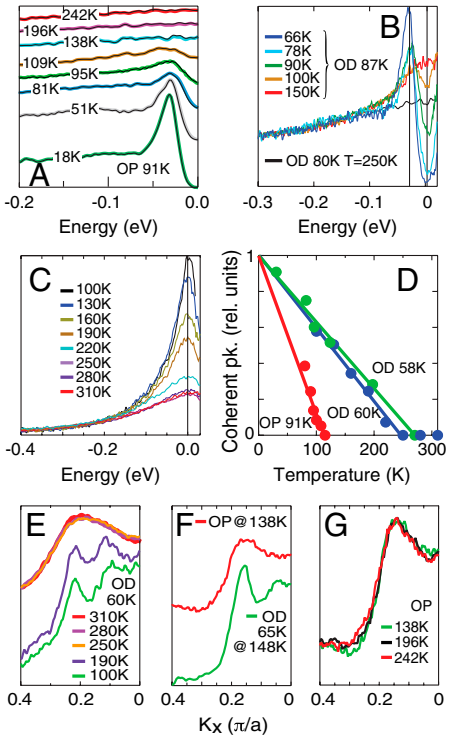

Fig. 3. Fermi function divided spectra. (*A*) Antinodal spectra for two optimally doped samples, $\delta = 0.16$, showing sharp peaks with an energy gap (green curves) below T^*, but broad gapless spectra (purple curve) above T^*. Colored lines show Fermi function-divided data, with symmetrized data superimposed as sharp black lines. (*B*) Spectra for an overdoped sample, $\delta = 0.183$, showing that, unlike in *A*, the spectral gap is lost above 100 K, whereas the sharp peak persists to higher temperature. (*C*) Data for an overdoped $\delta = 0.224$ sample. The sharp spectral peak decreases in intensity with increasing temperature. By $T = 250$ K, the spectral line shape is broad and temperature independent. (*D*) Linearly decreasing intensity of the sharp spectral peak relative to the broad Lorentzian with increasing T for three values of δ. T_{coh} is where this intensity reaches zero. (*E*) Momentum distribution curves (MDCs) for an overdoped $\delta = 0.224$ sample, showing that a qualitative change in spectral shape occurs near T_{coh}. (*F*) Comparison of the MDC of an OP doped sample, to that of an OD sample at a similar T. (*G*) T-independence of the spectral shape for an OP sample above T_{coh}.

For T_{coh}, we need to identify where the sharp peak disappears. We find that we can model the broad, incoherent part of the spectrum with a Lorentzian centered at E_F, and the sharp, coherent piece with a Gaussian (for details, see *SI Appendix*). In Fig. 3*D*, we plot the height of the sharp component of the spectra above that of the constant Lorentzian. One clearly sees a linear decrease with T, from which we determine T_{coh}. T_{coh} can also be observed in plots of the angle-resolved photoemission (ARPES) signal as a function of momentum for a fixed energy, the momentum distribution curves shown in Fig. 3 *E*–*G*. In Fig. 3*E*, we show that a significant change in width occurs upon crossing T_{coh}, which clearly indicates that this is not a simple temperature broadening effect. The spectra remain relatively unchanged both below and above T_{coh}, with significant changes limited to temperatures close to T_{coh}. Furthermore, T_{coh} is strongly doping dependent. In Fig. 3*F*, we show spectra at similar T for an optimally doped sample and an overdoped one with $T_c = 65$ K, showing that the spectral widths depend on the region of the phase diagram, and not simply the temperature. This is emphasized in Fig. 3*G*, where no spectral changes are observed in the strange metal region over a wide range in temperature.

The phase diagram shown in Fig. 4 summarizes our results. The solid dots are based on the antinodal spectra and are color coded to correspond to the four different regions in the normal state phase diagram. These correspond to antinodal spectra that

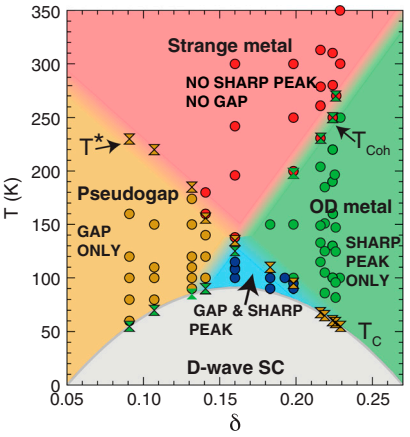

Fig. 4. Electronic phase diagram of $Bi_2Sr_2CaCu_2O_{8+\delta}$ versus hole doping, δ. Brown dots indicate incoherent gapped spectra, blue points coherent gapped spectra, green dots coherent gapless spectra, and red dots incoherent gapless spectra. The brown double triangles denote T^*, and the green double triangles T_{coh}. T_c denotes the transition temperature into the superconducting state (shaded gray and labeled D-wave SC).

are: (*i*) incoherent and gapped (brown dots), in the underdoped pseudogap region, (*ii*) incoherent and gapless (red dots), in the high-temperature strange metal, (*iii*) coherent and gapless (green dots), in the overdoped metal, and finally (*iv*) coherent and gapped (blue dots), in the triangular region above optimal doping formed as a result of the crossing of T^* and T_{coh}. In addition, we also plot T^* and T_{coh} as defined above by double triangles. We emphasize that, below T_c, we find coherent and gapped antinodal spectra for all doping values, even for very underdoped samples (6).

An earlier ARPES experiment showed the appearance of dichroism below a temperature equivalent to the T^* measured here (19), as did subsequent neutron scattering experiments that detected intraunit cell magnetic order (20, 21), both of which identify T^* as a phase transition. However, the present experiments do not measure an order parameter. Moreover, it is not clear that the large energy gap is due to magnetism. We therefore limit ourselves to calling T^* a "temperature scale."

Although heat capacity (22) and more recent transport studies (23) have suggested Fig. 1*B*, transport represents a single static (dc) quantity. On the other hand, photoemission being an energy and momentum resolved probe, allows one to uniquely separate the influence of coherence, a spectral gap, and their momentum dependence. In further support of Fig. 4, we note that the high-doping side of the blue triangle near optimal doping, characterized by gapped and coherent spectra above T_c, has also been inferred from the T dependence of scanning tunneling spectra (24). To our knowledge, however, the full triangular region has not been identified before. Although at first sight this triangular region seems similar to the region where diamagnetism is observed above T_c (25), the latter has a larger extent over the phase diagram than the former. This is not a surprise because we are measuring single particle coherence, whereas the diamagnetism is a measure of superconducting fluctuations.

Our experimental finding that the two temperature scales intersect is not consistent with a single quantum critical point near optimal doping, although more complicated quantum critical scenarios cannot be ruled out. For instance, quantum critical points exist at the ends of the dome (26, 27). In our data, Fig. 4, superconductivity only emerges below both T^* and T_{coh}. And, optimal superconductivity emerges from a coherent, gapped, normal state. Hence, our results are more naturally consistent with theories of superconductivity for doped Mott insulators, as illustrated in Fig. 1*C*. We believe these results represent an

important step forward in solving the highly challenging problem of high-temperature superconductivity.

This work was supported by the National Science Foundation under Grant DMR-0606255 (to J.C.C.), and NSF-DMR 0706203 (to M.R.). Work was performed at the Synchrotron Radiation Center, University of Wisconsin (Award DMR-0537588). The work at Argonne National Laboratory was supported by UChicago Argonne, LLC, Operator of Argonne National Laboratory. Argonne, a US Department of Energy, Office of Science laboratory is operated under Contract DE-AC02-06CH11357 (to S.R., A.K., M.R.N., and J.C.C.).

1. Schrieffer JR (1999) *Theory of Superconductivity* (Perseus Books, New York).
2. Ding H, et al. (1996) Spectroscopic evidence for a pseudogap in the normal state of underdoped high-Tc superconductors. *Nature* 382:51–54.
3. Loeser AG, et al. (1996) Excitation gap in the normal state of underdoped $Bi_2Sr_2CaCu_2O_{8+\delta}$. *Science* 273:325–329.
4. Kaminski A, et al. (2003) Crossover from coherent to incoherent electronic excitations in the normal state of $Bi_2Sr_2CaCu_2O_{8+\delta}$. *Phys Rev Lett* 90:207003.
5. Valla T, et al. (2000) Temperature dependent scattering rates at the Fermi surface of optimally doped $Bi_2Sr_2CaCu_2O_{8+\delta}$. *Phys Rev Lett* 85:828–831.
6. Chatterjee U, et al. (2010) Observation of a d-wave nodal liquid in highly underdoped $Bi_2Sr_2CaCu_2O_{8+\delta}$. *Nat Phys* 6:99–103.
7. Norman MR, et al. (1998) Destruction of the Fermi surface in underdoped high-T_c superconductors. *Nature* 392:157–160.
8. Varma CM (2006) Theory of the pseudogap state of the cuprates. *Phys Rev B Condens Matter Mater Phys* 73:155113.
9. Sachdev S (2010) Where is the quantum critical point in the cuprate superconductors? *Phys Status Solidi B* 247:537–543.
10. Varma CM, et al. (1989) Phenomenology of the normal state of the Cu-O high-temperature superconductors. *Phys Rev Lett* 63:1996–1999.
11. Anderson PW (1987) The resonating valence bond state in La_2CuO_4 and superconductivity. *Science* 235:1196–1198.
12. Suzumura Y, Hasegawa Y, Fukuyama H (1988) Mean field theory of RVB and superconductivity. *J Phys Soc Jpn* 57:2768–2778.
13. Kotliar G (1988) Resonating valence bonds and d-wave superconductivity. *Phys Rev B Condens Matter Mater Phys* 37:3664–3666.
14. Lee PA, Nagaosa N, Wen X-G (2006) Doping a Mott insulator: Physics of high-temperature superconductivity. *Rev Mod Phys* 78:17–85.
15. Timusk T, Statt B (1999) The pseudogap in high-temperature superconductors: An experimental survey. *Rep Prog Phys* 62:61–122.
16. Valla T, et al. (2002) Coherence-incoherence and dimensional crossover in layered strongly correlated metals. *Nature* 417:627–630.
17. Matsui H, et al. (2003) BCS-like bogoliubov quasiparticles in high-T_c superconductors observed by angle resolved photoemission spectroscopy. *Phys Rev Lett* 90:217002.
18. Kanigel A, et al. (2006) Evolution of the pseudogap from Fermi arcs to the nodal liquid. *Nat Phys* 2:447–451.
19. Kaminski A, et al. (2002) Spontaneous breaking of time-reversal symmetry in the pseudogap state of a high-T_c superconductor. *Nature* 416:610–613.
20. Fauque B, et al. (2006) Magnetic order in the pseudogap phase of high T_c superconductors. *Phys Rev Lett* 96:197001.
21. Li Y, et al. (2008) Unusual magnetic order in the pseudogap region of the superconductor $HgBa_2CuO_{4+\delta}$. *Nature* 455:372–375.
22. Tallon JL, Loram JW (2001) The doping dependence of T^*—what is the real high-T_c phase diagram? *Physica C* 349:53–68.
23. Hussey NE, et al. (2011) Dichotomy in the T-linear resistivity in hole-doped cuprates. *Philos Trans R Soc A* 369:1626–1639.
24. Gomes KK, et al. (2007) Visualizing pair formation on the atomic scale in the high-T_c superconductor $Bi_2Sr_2CaCu_2O_{8+\delta}$. *Nature* 447:569–572.
25. Li L, et al. (2010) Diamagnetism and Cooper pairing above T_c in cuprates. *Phys Rev B Condens Matter Mater Phys* 81:054510.
26. Broun DM, et al. (2007) Superfluid density in a highly underdoped $YBa_2Cu_3O_{6+y}$ superconductor. *Phys Rev Lett* 99:237003.
27. Hetel J, Lemberger TR, Randeria M (2007) Quantum critical behavior in the superfluid density of strongly underdoped ultrathin copper oxide films. *Nat Phys* 3:700–702.